Afyon Kocatepe Üniversitesi Fen ve Mühendislik Bilimleri Dergisi
Afyon Kocatepe University – Journal of Science and Engineering
https://dergipark.org.tr/tr/pub/akufemubid

Araştırma Makalesi / Research Article
e-ISSN: 2149-3367
DOI: https://doi.org/10.35414/akufemubid.1709026
AKÜ FEMÜBİD **26** (2026) 011102 (23-35)
AKU J. Sci. Eng. **26** (2026) 011102 (23-35)

Investigation of Gamma Shielding Characteristics of Al_2O_3/NbC Composites via Experimental Measurements and Phy-X/PSD Analysis

Makale Bilgisi / Article Info
Alındı/Received: 29.05.2025
Kabul/Accepted: 18.09.2025
Yayımlandı/Published: 03.02.2026

Al_2O_3/NbC Kompozitlerinin Gama Zırhlama Özelliklerinin Deneysel Ölçümler ve Phy-X/PSD Analizi Yoluyla İncelenmesi

Kadir GÜNOĞLU*

Isparta Uygulamalı Bilimler Üniversitesi, Teknik Bilimler Meslek Yüksekokulu, Isparta-Türkiye

Abstract

This study explores the gamma radiation shielding performance of alumina (Al_2O_3)-based composites reinforced with varying weight fractions of niobium carbide (NbC). The evaluation was conducted through a combination of experimental measurements and theoretical simulations. Key radiation shielding parameters—including the linear attenuation coefficient (LAC), half value layer (HVL), tenth value layer (TVL), mean free path (MFP), and radiation protection efficiency (RPE)—were experimentally determined at photon energies of 0.662, 1.173, and 1.332 MeV using a gamma spectroscopy system. It was observed that the experimentally determined LAC values increased as the NbC ratio in the composite increased. The LAC values varied between 0.269 and 0.392 cm^{-1} for 0.662 MeV, 0.223 and 0.271 cm^{-1} for 1.173 MeV and 0.189 and 0.250 cm^{-1} for 1.332 MeV. The MFP, HVL and TVL parameters, which changed inversely proportional to the LAC values, decreased with increasing NbC ratio. In addition to the experimentally found parameters, theoretical calculations of the effective atomic number (Zeff), effective electron density (Neff) and exposure accumulation factor (EBF) parameters were made in the wide energy range between 0.015 and 15 MeV using the Phy-X/PSD software. The comparison between experimental and theoretical results revealed a high degree of consistency, validating the reliability of the computational model. Furthermore, the incorporation of NbC was found to significantly improve the gamma attenuation properties of the alumina matrix, primarily due to enhancements in density and atomic interaction probability. These findings highlight the potential of NbC-reinforced alumina composites for use in advanced radiation shielding applications, particularly in environments requiring lightweight and high-performance protective materials.

Anahtar Kelimeler: *Gamma radiation shielding, Alumina composites, Niobium carbide (NbC), gamma spectroscopy, Phy-X/PSD.*

Öz

Bu çalışma, alümina (Al_2O_3) esaslı kompozitlerin gamma radyasyonunun zırhlanma performansını niyobyum karbür (NbC) ile farklı ağırlık yüzdelerinde takviye edilmesi üzerine odaklanmaktadır. Değerlendirme, deneysel ölçümler ve teorik simülasyonların kombinasyonuyla gerçekleştirilmiştir. Ana radyasyon zırhlama parametreleri, lineer zayıflama katsayısı (LAC), yarı değer katmanı (HVL), onda bir değer katmanı (TVL), ortalama serbest yol (MFP) ve radyasyon koruma verimliliği (RPE), gamma spektroskopi sistemi kullanılarak 0.662, 1.173 ve 1.332 MeV foton enerjilerinde deneysel olarak belirlenmiştir. Deneysel olarak belirlenen LAC değerlerinin kompozit içerisindeki NbC oranı arttıkça arttığı gözlenmiştir. LAC değerleri 0.662 MeV için 0.269 ile 0.392 cm^{-1}, 1.173 MeV için 0.223 ile 0.271 cm^{-1} ve 1.332 MeV için 0.189 and 0.250 cm^{-1} arasında değişmiştir. LAC değerleri ile ters orantılı olarak değişen MFP, HVL ve TVL parametreleri artan NbC oranına göre düşmüştür. Deneysel olarak bulunan parametrelere ek olarak Phy-X/PSD yazılımı kullanılarak 0.015 ile 15 MeV arasındaki geniş enerji aralığında etkili atom numarası (Zeff), etkili elektron yoğunluğu (Neff) ve maruziyet birikim faktörü (EBF) parametrelerinin teorik hesaplamaları yapılmıştır. Deneysel ve teorik sonuçların karşılaştırılması, hesaplama modelinin güvenilirliğini doğrulayan yüksek derecede tutarlılık göstermiştir. Ayrıca, NbC'nin alümina matrisine katılmasının, özellikle yoğunluk ve atomik etkileşim olasılığında sağladığı iyileştirmeler nedeniyle gamma zayıflatma özelliklerini önemli ölçüde artırdığı bulunmuştur. Bu bulgular, NbC takviyeli alümina kompozitlerinin hafif ve yüksek performanslı koruyucu malzemeler gerektiren ileri düzey gamma radyasyonu zırh uygulamalarında potansiyelini ortaya koymaktadır.

Keywords: *Gama radyasyon zırhlama, Alümina kompozitler, Niyobyum karbür (NbC), gama spektroskopisi, Phy-X/PSD.*

1. Introduction

Ionizing radiation is widely utilized in diverse fields such as nuclear energy, industry, space exploration, and especially medicine, where it plays a vital role in diagnostic and therapeutic procedures including radiography, computed tomography (CT), nuclear medicine, and radiotherapy applications.

In industrial sectors, radiation is used for sterilization, food preservation, material testing, and power generation. Despite its substantial benefits, ionizing

*Sorumlu Yazar/Corresponding Author: Kadir GÜNOĞLU e-posta/e-mail: kadirgunoglu@isubu.edu.tr

radiation poses significant health and environmental hazards due to its high energy and ability to ionize atoms, potentially leading to molecular alterations and cellular damage (UNSCEAR 2010. IAEA 2018).

Given the irreplaceable role of ionizing radiation in modern technology, its use cannot be entirely eliminated. Instead, the emphasis must be placed on reducing radiation risks through effective protection strategies. The three fundamental principles of radiation protection are minimizing exposure time, maximizing distance from the source, and implementing appropriate shielding. Among these, shielding is considered the most versatile and widely applicable strategy, particularly in environments where continuous exposure is inevitable (NCRP 2000, Li et. al. 2024).

Radiation shielding involves placing a material between the source of radiation and the target, effectively reducing radiation intensity through mechanisms such as absorption or scattering. The efficiency of a shielding material is determined by its interaction with the specific type of radiation—alpha particles can be blocked by paper, beta particles by plastic or aluminum, while high-energy photons like gamma rays require dense, high atomic number (Z) materials such as lead, bismuth, or tungsten (Ammar et. al. 2022, Kumar 2017). For neutron radiation, hydrogen-rich materials such as water, polyethylene, or borated substances are more appropriate due to their neutron moderating properties (Kaur et. al. 2016). However, the selection of shielding materials is not solely based on radiation attenuation performance. Depending on the application, additional factors such as weight, flexibility, toxicity, cost, mechanical strength, thermal stability, and environmental compatibility must be considered. For instance, in aerospace or medical applications, lightweight and non-toxic materials are essential. Moreover, shielding materials must ensure long-term stability under continuous radiation exposure without degradation (Sayyed et. al. 2019)

In response to these demands, considerable research has focused on the development of advanced shielding materials, including polymer-based composites, heavy metal oxide-enriched glass systems, nanostructured materials, and ceramic matrices. These materials often combine radiation attenuation properties with improved mechanical and chemical characteristics, providing an effective and safer alternative to traditional shielding solutions like lead, which poses significant environmental and health concerns (Al-Buriahi et. al. 2021). With the rapid progression of modern technology and the growing incorporation of radiation-emitting systems in medical, industrial, and energy-related fields, the demand for advanced radiation shielding materials has become increasingly urgent. In response, significant research efforts have been devoted to the development of next-generation shielding materials capable of effectively reducing the harmful effects of ionizing radiation. These materials are typically formulated from a wide range of substances, including composites (comprising various mixtures and compounds) (AL Misned et. al. 2023, Atashi et. al. 2018, Gunoglu et. al. 2024, Oto et. al. 2024) metal alloys (Gul et. al. 2022, Alzahrani et. al. 2022, Alshahrani et. al. 2021, Almuqrin et. al. 2021), specialized concretes (Akkurt et. al. 2012, Akkurt and Gunoglu 2021, Mansour et. al. 2023, Zayed et. al. 2024), glasses, and polymer-based systems (Afshar et. al. 2019, Kaçal et. al. 2020. Alsayed et. al. 2020. Mansy et. al. 2024). Investigations in this field frequently involve a dual approach, combining experimental methods with theoretical modeling to comprehensively assess key radiation shielding parameters such as attenuation coefficients, buildup factors, and protection efficiencies (Turhan et. al. 2022, Alzahrani et. al. 2023, Güler et. al. 2024) These studies play a vital role in guiding the design and optimization of high-performance shielding solutions for diverse practical applications.

This study focuses on the investigation of gamma radiation shielding properties of alumina-based composites reinforced with different weight percentages of niobium carbide (NbC), specifically 0%, 5%, 10%, and 20%. Initially, the LACs of the composite samples were experimentally determined using gamma spectroscopy system with NaI(Tl) detector. Based on these measurements, essential shielding parameters—including MFP, HVL, TVL, RPE —were subsequently calculated. In parallel, theoretical evaluations of the same parameters were conducted using the Phy-X/PSD software, which accounts for the elemental composition and measured densities of the samples. A comparative analysis between the experimental results and theoretical predictions was performed to assess the level of agreement and validate the reliability of the computational approach.

2. Materials and Methods

2.1 Preparation of Composite Samples

In this study, alumina-based composites reinforced with different weight fractions of niobium carbide (NbC) were fabricated. High-purity Al_2O_3 powder (≥99%) was used as the matrix material, while NbC powder (≥99% purity, <45 µm particle size) served as the reinforcement. Five

different compositions were prepared containing 0, 5, 10, 20 and 30 wt% NbC.

Initially, the predetermined amounts of Al_2O_3 and NbC powders were accurately weighed and mixed using a ball milling process for 6 hours at 300 rpm in an ethanol medium to ensure homogeneous dispersion. Zirconia balls were used as the milling media, and intermittent stirring was performed to prevent agglomeration during the mixing process.

The resulting slurry was dried in an oven at 80 °C for 24 hours. The dried powder mixture was then uniaxially compacted into cylindrical molds and subsequently subjected to cold isostatic pressing (CIP) at 200 MPa to form green compacts. The thickness of the resulting samples was measured as 1 cm. After pressing, the samples were sintered at 1500°C in a controlled atmosphere for 2 hours.

Composite samples were coded as ALNBC0 (alumina), ALNBC5 (%5 NbC), ALNBC10 (%10 NbC) ALNBC20 (%20 NbC) and ALNBC30 (%30 NbC). Table 1 shows the sample codes, alumina (Al_2O_3) - niobium carbide (NbC) ratios and densities of composites.

Table 1. Alumina (Al_2O_3) - niobium carbide (NbC) ratios ratios and densities of composites

Composite Code	Combination (wt %)		Density ($g.cm^{-1}$)
	Alumina (Al_2O_3)	Niobium Carbide (NbC)	
ALNBC0	100	0	3.75
ALNBC5	95	5	3.92
ALNBC10	90	10	4.11
ALNBC20	80	20	4.52
ALNBC30	70	30	4.96

2.2 Gamma ray attenuation measurements

In the first stage of this study, LAC values of composites produced by adding varying amounts of niobium carbide (NbC) to alumina (Al_2O_3) were measured experimentally. For the measurements, a gamma ray spectrometry system equipped with a 3*3 inch NaI(Tl) scintillation detector (Canberra, Model-802) was employed to determine the linear attenuation coefficients (LAC) of the samples at gamma energies of 0.662, 1.173 and 1.332 MeV. These gamma photons were emitted from point sources of ^{137}Cs and ^{60}Co. The spectrometry setup was completed by integrating the detector with a Multi-Channel Analyzer (MCA), High Voltage (HV) power supply, amplifier, and other essential electronics to ensure accurate signal acquisition and processing (see Figure 1). The MAESTRO-32 software was used for spectrum acquisition, processing, and analysis.

Compared to charged particles, the interactions of photons (such as gamma rays and X-rays) with matter exhibit fundamentally different behaviors. When a photon beam enters a material, three primary outcomes are possible: a portion of the photons is absorbed, another portion is transmitted through the material without interaction, and the remainder is scattered, particularly for lower-energy photons. These processes are probabilistic and strongly depend on several factors, including the energy of the incident photons, the atomic composition and density of the shielding material, and the experimental conditions.

Materials with higher photon attenuation capabilities are generally preferred for shielding applications, especially when minimizing the thickness and weight of the shield is desirable. A crucial concept used to describe the attenuation of photon beams in matter is the Beer–Lambert law, also known as the law of exponential attenuation. This law mathematically describes the reduction in photon intensity as a function of the absorber's thickness: (Bashter 1997).

$$I = I_0 e^{-\mu x} \quad (1)$$

$$LAC\ (\mu, cm^{-1}) = \frac{1}{x} Ln \frac{I_0}{I} \quad (2)$$

Where I and I_0 symbolize the gamma rays coming and passing through the material, respectively. μ is the LAC value. x means shielding material thickness.

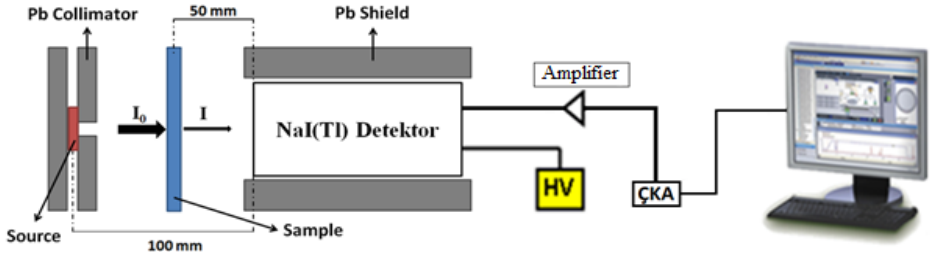

Figure 1. Schematic view of the experimental setup.

The mass attenuation coefficient (MAC), represented as μ/ρ and measured in cm^2/g, is a key parameter that quantifies how effectively a material can attenuate gamma or X-ray photons relative to its mass. It is obtained by dividing the LAC (μ, in cm^{-1}) by the material's density (ρ, in g/cm^3) (Gunoglu et. al.2021).

In the case of composite materials, the MAC for a specific photon energy can be estimated using the mixture rule, which involves calculating the weighted average of the MAC values of each constituent element based on their respective proportions in the composite.

$$\mu_m = (\mu/\rho) = \sum_i w_i\,(\mu/\rho)_i \quad (3)$$

In this context, wi and (μ/ρ)i represent the weight fraction and the MAC of the i-th element in the chemical composition of the shielding material, respectively. The weight fraction w_i of each element can be calculated using the following equation:

$$w_i = \frac{A_i a_i}{\sum_i A_i a_i} \quad (4)$$

Here, A_i represents the atomic weight of the *i-th* element, and a_i denotes the number of atoms of the *i-th* element in the chemical formula unit of the shielding material.

The MFP, also known as the relaxation length (λ), refers to the average distance a gamma photon travels in a material before undergoing an interaction. It is typically expressed in centimeters and can be calculated using the inverse of the LAC (μ) as: (Gunoglu 2024):

$$MFP\ (\lambda, cm) = \frac{1}{LAC} \quad (5)$$

The HVL is defined as the thickness of a material necessary to reduce the intensity of incoming gamma radiation to half of its original value. It serves as an important parameter for evaluating the shielding efficiency of a material against gamma photons at different energy levels. A smaller HVL value indicates better attenuation capability, especially for lower-energy photons with limited penetrating power.

The HVL, denoted as $T_1/_2$ and measured in centimeters, can be determined using the following equation: (Gunoglu 2024).

$$HVL\left(T_{1/2}, cm\right) = \frac{Ln2}{LAC} \quad (6)$$

The TVL, also represented as $T_1/_{10}$ and measured in centimeters, refers to the thickness of a shielding material required to decrease the intensity of incident gamma radiation to 10% of its initial value. In other words, it corresponds to a 90% reduction in radiation intensity. Similar to the HVL, the TVL is a crucial parameter for evaluating a material's radiation shielding capability, particularly in scenarios requiring higher degrees of attenuation. (Gunoglu 2024).

$$TVL\left(T_{1/10}, cm\right) = \frac{Ln10}{LAC} \quad (7)$$

Radiation Shielding Efficiency (RPE) is one of the key parameters used to evaluate the shielding performance of a material against ionizing radiation. It quantifies the material's ability to attenuate incident radiation and is expressed as a percentage reduction in radiation intensity after passing through the shielding medium (Gunoglu et. al.2024).

$$RPE(\%) = \left(\frac{I_0 - I}{I_0}\right) x100 \quad (8)$$

A higher RPE value indicates better shielding performance. This parameter is particularly useful for comparing different materials or different thicknesses and compositions of the same material under identical radiation exposure conditions.

In order to assess the radiation shielding performance of the prepared samples, various attenuation parameters were computed using the Phy-X/PSD software (Şakar et. al. 2020). This open-access computational tool provides precise and dependable evaluations of radiation interaction properties over a broad spectrum of photon energies. In this work, calculations were carried out for photon energies ranging from 0.015 MeV to 15 MeV for each sample formulation. Phy-X/PSD determines essential shielding characteristics based on the elemental makeup and experimentally measured density of the samples. Among the parameters calculated are LAC, MAC, HVL, TVL, MFP, Z_{eff}, N_{eff}, EBF. These parameters play a crucial role in describing the material's effectiveness in attenuating gamma rays within the specified energy interval.

The Z_{eff} and N_{eff} are key parameters derived from the total atomic (σ_t) and electronic (σ_e) cross-sections. These values are instrumental in characterizing the interaction of photons with matter and serve as vital indicators of a material's radiation shielding capability. By capturing both atomic and electronic scale interactions, Z_{eff} and N_{eff} offer a more comprehensive understanding of the attenuation behavior of composite and heterogeneous materials across a wide photon energy range (Tekin et. al. 2020).

$$\sigma_t = \frac{\mu_m N}{N_A},\ \sigma_e = \frac{1}{N_A}\sum_i \frac{f_i N_i}{Z_i}(\mu_m)_i \quad (9)$$

$$Z_{eff} = \frac{\sigma_t}{\sigma_e} \quad (10)$$

$$N_{eff} = \frac{N_A}{N} Z_{eff} \sum_i n_i = \frac{\mu_m}{\sigma_e} \quad (11)$$

To evaluate the EBF for ALNBC samples reinforced with different weight fractions of NbC, it is first necessary to determine the equivalent atomic number (Z_{eq}) and the Geometric Progression (G-P) fitting parameters. The equivalent atomic number serves as a crucial descriptor, enabling the characterization of photon interaction behavior in a composite material as though it were a homogeneous single-element absorber.

To compute Z_{eq}, both the total MAC, $(\mu/\rho)_{total}$, and the Compton scattering partial MAC, $(\mu/\rho)_a C_{omp}$, must be obtained at the photon energy of interest. Once these coefficients are known, Z_{eq} can be determined through logarithmic interpolation between two elements with known atomic numbers (Z_1 and Z_2) using the following empirical formula (Singh et. al. 2008):

$$Z_{eq} = \frac{Z_1(logR_2 - logR) + Z_2(logR - logR_1)}{logR_2 - logR_1} \quad (12)$$

where

• Z_1 and Z_2 are the atomic numbers of elements for which the tabulated values of R_1 and R_2 bracket the calculated value of R.

• R_1 and R_2 are the corresponding Compton-to-total attenuation ratios for Z_1 and Z_2, respectively.

This interpolation method allows estimation of Z_{eq} for composite materials, which is then used to compute the G-P fitting parameters necessary for evaluating the EBF values over a range of energies and penetration depths (Tekin et. al. 2020).

$$P = \frac{P_1(logZ_2 - logZ_{eq}) + P_2(logZ_{eq} - logZ_1)}{logZ_2 - logZ_1} \quad (13)$$

where P_1 and P_2 represent the G-P fitting parameters associated with the atomic numbers Z_1 and Z_2, respectively. The calculations were carried out using G-P fitting parameters sourced from the ANSI/ANS-6.4.3 standard reference database, which provides validated data for exposure buildup factor computations across a wide range of materials and photon energies. (ANSI/ANS-6.4.3, 1991).

The G-P fitting parameters derived from the aforementioned equations can be used to estimate the EBF values for any shielding material (Singh et. al. 2008).

$$B(E,X) = 1 + \frac{b-1}{K-1}.(K^x - 1) \quad \text{for} K \neq 1 \quad (14)$$

$$B(E,X) = 1 + (b-1).x \quad \text{for} K = 1 \quad (15)$$

$$K(E,X) = cx^a + d.\frac{tanh\left(\frac{x}{X_k} - 2\right) - tanh(-2)}{1 - tanh(-2)} \text{for } x \leq 40MFP \quad (16)$$

where X denotes the depth of penetration, while E represents the initial gamma-ray energy. The G-P fitting parameters are expressed by the coefficients b,c,a,d, and Xk.

3. Results and Discussions

LAC values of ALNBC composite samples containing varying weight percentages of niobium carbide (NbC) were determined through both experimental measurements and theoretical calculations at three different gamma-ray energies. These energies were selected based on emissions from two distinct radioactive sources. The theoretical LAC values for each composite formulation were computed using the Phy-X/PSD software, which is widely utilized for photon interaction studies in shielding materials. A comparative analysis of the experimental and theoretical LAC results is presented in Table 2. Furthermore, the table includes the relative deviation (RD) values, expressed as percentages, to evaluate the consistency between experimental data and theoretical predictions. The RD serves as a quantitative indicator of agreement and was calculated according to the following equation:

$$RD(\%) = \left(\frac{|LAC_{Exp.} - LAC_{\text{Phy-X/PSD}}|}{LAC_{Exp.}}\right) x100 \quad (17)$$

The RD values were found to range between 0.80% and 7.53%. These findings suggest that the discrepancies between the experimental and theoretical LAC values are relatively minor, indicating a strong agreement between the two data sets (Table 2.). The observed differences are primarily attributed to experimental uncertainties, such as variations in sample mass and thickness, as well as fluctuations in the measured incident (I_0) and transmitted (I) photon intensities.

Table 2. Experimental and theoretical LAC values for ALNBC composites.

Samples	0.662 MeV			1.173 MeV			1.332 MeV		
	Exp. (cm^{-1})	Phy-X/PSD (cm^{-1})	RD	Exp.	Phy-X/PSD (cm^{-1})	RD	Exp.	Phy-X/PSD (cm^{-1})	RD
ALNBC0	0.269±0.009	0.285	5.82	0.223±0.007	0.217	2.91	0.189±0.006	0.203	7.53
ALNBC5	0.288±0.008	0.297	3.34	0.235±0.008	0.226	3.85	0.207±0.007	0.211	2.04
ALNBC10	0.325±0.008	0.311	4.12	0.250±0.007	0.236	5.66	0.233±0.007	0.221	5.17
ALNBC20	0.356±0.01	0.342	4.12	0.267±0.009	0.258	3.56	0.243±0.009	0.242	0.80
ALNBC30	0.392±0.013	0.374	4.49	0.271±0.011	0.281	3.75	0.250±0.009	0.263	5.26

As illustrated in Figure 2, the LAC values for all samples are influenced by both the energy of the incident gamma photons and the NbC content within the composite. Specifically, LAC values tend to decrease with increasing gamma-ray energy, in accordance with the well-established attenuation behavior of materials. Conversely, an increase in NbC content leads to a corresponding increase in LAC values, highlighting the positive contribution of NbC to gamma attenuation performance.

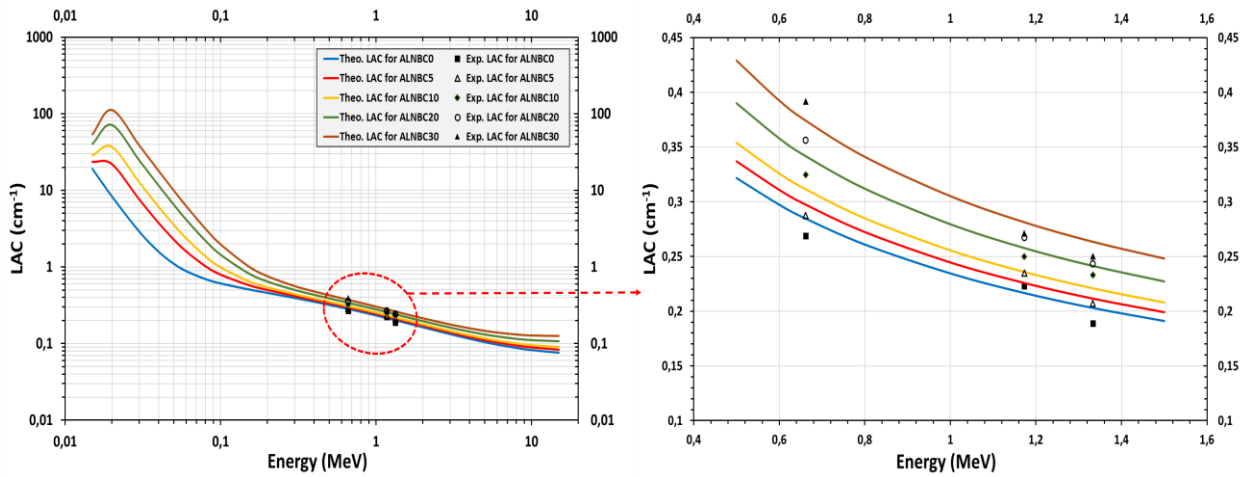

Figure 2. Experimental and theoretical LAC results measured at different gamma energies for ALNBC samples.

Moreover, the close correspondence between the experimental and theoretical data shown in Figure 2 further validates the accuracy and reliability of the experimental setup employed in this study.

Since the gamma-ray linear attenuation coefficient (LAC) is strongly dependent on material density, the experimental LAC values of the ALNBC samples are presented as a 3D surface plot in Figure 3, with respect to both gamma-ray energy and sample density. As shown in the figure, the density of the samples increases with the addition of NbC to the alumina matrix. Consequently, higher material density leads to an increase in the experimentally measured LAC values. Among the investigated samples, the ALNBC30 composite, which contains 30 wt% NbC, exhibited the highest LAC value, confirming the positive influence of NbC content on gamma attenuation performance.

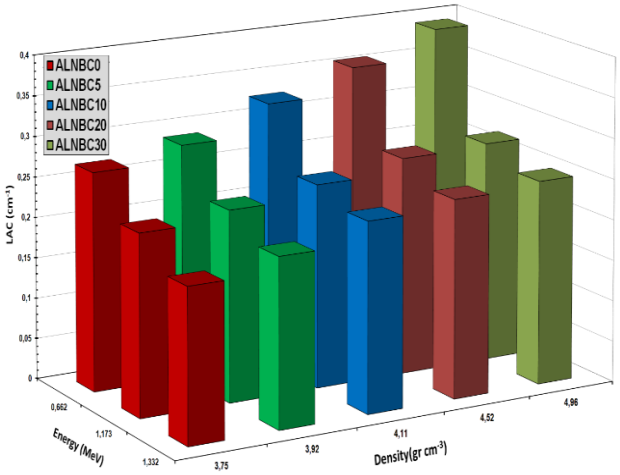

Figure 3. Change in measured LAC values depending on the composite density

In Table 3, the mass attenuation coefficient results obtained in this study are compared with those reported in previous studies on different aluminum alloys. Manjunatha et al. reported only the mass attenuation coefficients of different aluminum alloys in their study. When compared with the present results, it is evident that increasing the NbC content in alumina leads to higher mass attenuation coefficients than those of the aluminum alloys.

Similarly, Gökmen et al. investigated the mass attenuation coefficients of Alumix 231 (Al-14Si-2.5Cu-0.5 Mg (wt%)) and Alumix 13 (Al-4.5Cu-0.5Mg-0.1Si (wt%)) aluminum matrix composites reinforced with different amounts of B_4C. They reported that the mass attenuation coefficient increased with higher B_4C content.

Akman et al. examined the photon shielding performance of four alloy (Ag92.5/Cu7.5, Ag72/Cu28, Pd94/Cr6 and Pd60/Cu40) samples in their study. The results corresponding to the gamma-ray energies used in the present work are summarized in Table 3. A comparison of the findings reveals that while the mass attenuation coefficient (MAC) of pure alumina was comparable to those of the alloys, the incorporation of increasing amounts of NbC into the alumina matrix led to superior shielding performance relative to the those alloys.

Alzahrani et al. conducted a theoretical investigation into the radiation shielding characteristics of various nickel-, iron-, lead-, and tungsten-based alloys. When compared with the mass attenuation coefficient (MAC) values obtained in the present study, it was observed that the MACs were comparable to those of nickel- and iron-based alloys, whereas lead- and tungsten-based alloys exhibited significantly higher MAC values. This enhancement is primarily attributed to the higher densities and atomic numbers of lead and tungsten, which result in greater photon interaction probabilities.

Table 3. Comparison of our mass attenuation coefficient results with some other aluminum studies.

Samples	Energy (MeV)			References
	0.662	1.173	1.332	
ALNBC0	0.0717	0.0595	0.0503	Present Work
ALNBC5	0.0734	0.0599	0.0528	
ALNBC10	0.0790	0.0608	0.0567	
ALNBC20	0.0816	0.0619	0.0577	
ALNBC30	0.0823	0.0622	0.0587	
AL 47	0.0732	0.0584	0.0526	Manjunatha et. al. 2019
AL 32S	0.0756	0.0592	0.0546	
Al Si 43	0.0756	0.0586	0.0536	
Ferrosilicon	0.0786	0.0608	0.0552	
Al 355	0.0752	0.0596	0.0532	
Al 356	0.0696	0.0589	0.0532	
Al A 355	0.0742	0.0595	0.0528	
Alumix 231+%5B4C	0.0745	0.0568	0.0533	Gökmen et. al. 2020
Alumix 231+%10B4C	0.0744	0.0567	0.0532	
Alumix 231+%15B4C	0.0743	0.0566	0.0531	
Alumix 13+%5B4C	0.0741	0.0565	0.053	
Alumix 13+%10B4C	0.0740	0.0564	0.0529	
Alumix 13+%15B4C	0.0739	0.0563	0.0528	
Ag72/Cu28	0,0731	0,0521	0,0489	Akman et. al. 2019
Ag92,5/Cu7,5	0,0735	0,0539	0,0481	
Pd94/Cr6	0,072	0,0524	0,049	
Pd60/Cu40	0,0715	0,0526	0,0503	
Ni-based	0,0754	0,0561	0,0537	Alzahraniet. al. 2022
Fe-based	0,0732	0,0547	0,0528	
Pb-based	0,1056	0,0601	0,0565	
W-based	0,0964	0,0579	0,0544	

The linear attenuation coefficient (LAC) values were obtained experimentally at gamma-ray energies of 0.662 MeV, 1.173 MeV, and 1.332 MeV. Based on these values, the mean free path (MFP) for all alumina–niobium carbide (ALNBC) composites was calculated using Equation 5. The MFP results reflect the effects of both photon energy and NbC content. These values are presented in Figure 4.

As shown in the figure, MFP values increase with higher gamma-ray energy. This indicates that high-energy photons travel longer distances due to lower interaction probability. In contrast, low-energy gamma rays have shorter MFP values because they interact more easily with the material.

Among all the samples, the ALNBC0 composite (containing no NbC) shows the highest MFP values, corresponding to its relatively lower attenuation capacity. As the NbC content increases, the MFP values decrease. This shows that higher NbC content improves photon interaction. The effect is mainly due to the increased density and atomic number from the NbC reinforcement.

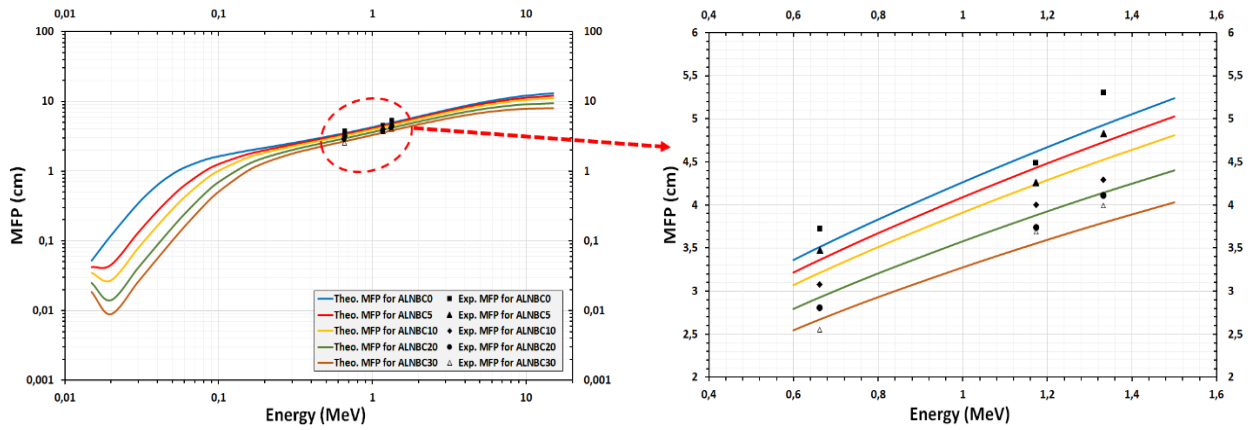

Figure 4. MFP results for ALNBC samples.

The HVL and TVL thicknesses of the ALNBC composite samples were derived using Equations 6 and 7, respectively, based on the experimentally measured LACs. These shielding parameters are critical indicators of a material's effectiveness in attenuating gamma radiation. The calculated HVL and TVL values are

presented in Figures 5 and 6, respectively, illustrating their dependence on both gamma-ray energy and the compositional variation of NbC within the composite matrix.

As observed in the figures, both HVL and TVL values increase with increasing gamma-ray energy, which is attributed to the greater penetration capability of high-energy photons. Conversely, increasing the NbC content in the composite results in a decrease in both HVL and TVL values, indicating enhanced attenuation performance. Among all samples, the ALNBC0 composite (without NbC) exhibits the highest HVL and TVL values at all investigated energies, reflecting its lower shielding efficiency. In contrast, the ALNBC30 sample, containing 30 wt% NbC, demonstrates the lowest HVL and TVL values.

These results clearly demonstrate that the incorporation of NbC markedly enhances the gamma-ray shielding performance of alumina-based composites. This improvement is primarily attributed to the increase in both material density and effective atomic number resulting from the presence of NbC as a reinforcing phase.

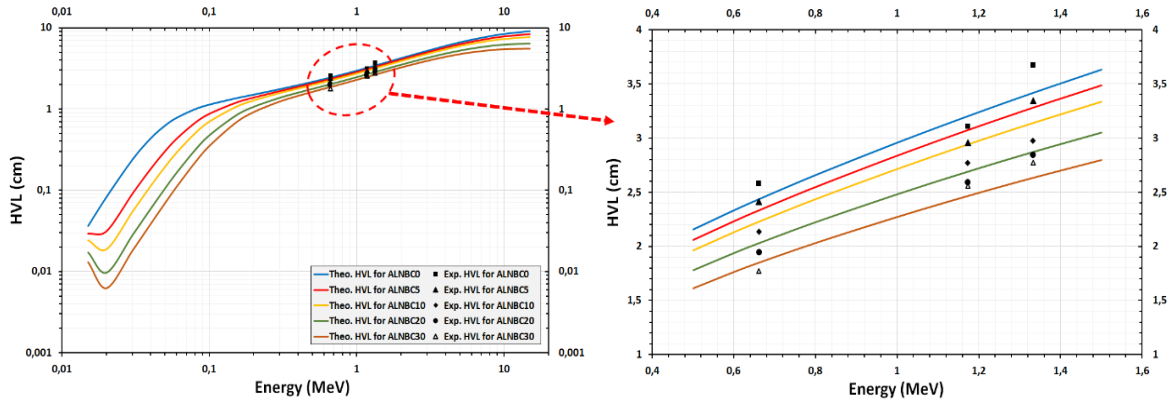

Figure 5. HVL results for ALNBC samples.

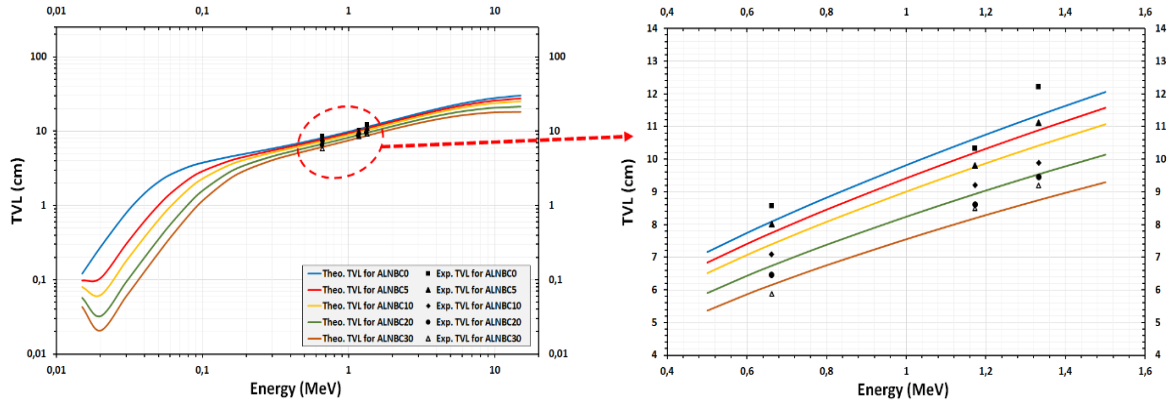

Figure 6. TVL results for ALNBC samples.

The radiation protection efficiency (RPE) values, derived from the ratio of unattenuated (I_0) to attenuated (I) gamma-ray intensities based on experimental data, are presented in Figure 7 for all ALNBC composite samples. As shown in the figure, the ALNBC30 sample—containing 30 wt% NbC—exhibited the highest RPE value, signifying its superior gamma-ray shielding capability compared to the other NbC-reinforced compositions. Moreover, the RPE values display a clear decreasing trend with increasing photon energy, which is consistent with the general reduction in attenuation efficiency at higher gamma-ray energies due to lower interaction probabilities. In contrast, a positive correlation is observed between RPE and NbC content, confirming that the inclusion of higher NbC fractions enhances the radiation attenuation performance of the alumina-based composites.

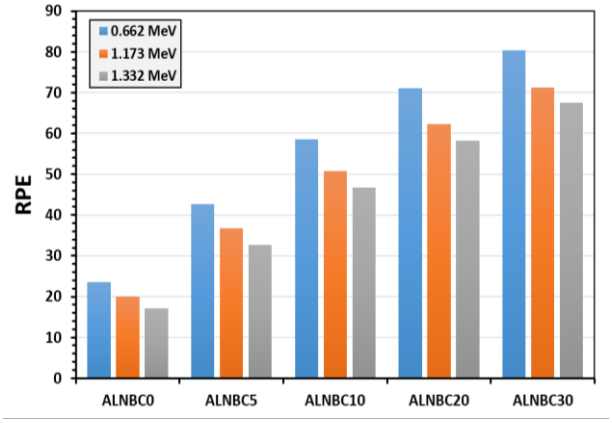

Figure 7. The RPE values for ALNBC samples

The theoretically determined effective atomic number (Z_{eff}) values for ALNBC samples with varying NbC content are presented in Figure 8. This figure illustrates the variation of Z_{eff} as a function of both photon energy and the chemical composition of the materials.

Across the studied samples, Z_{eff} values were found to range approximately from 10 to 35. The lowest Zeff was observed in pure alumina (ALNBC0) sample without any NbC additives, while the highest value was observed in ALNBC30 (containing 30% wt. NbC). It exhibited the highest Z_{eff}, which was attributed to the increased density and higher atomic number additives brought by NbC.

Theoretical Z_{eff} variation was analyzed in three energy ranges: low (0.015–0.4 MeV), medium (0.4–5 MeV), and high (≥ 5 MeV). In the low-energy range, Z_{eff} sharply declined due to the dominant photoelectric absorption, which strongly depends on atomic number. In the intermediate energy range, Z_{eff} remained relatively stable as Compton scattering became the prevailing interaction mechanism. At high photon energies (≥ 5 MeV), an increase in Z_{eff} was noted, corresponding to the onset and dominance of the pair production process.

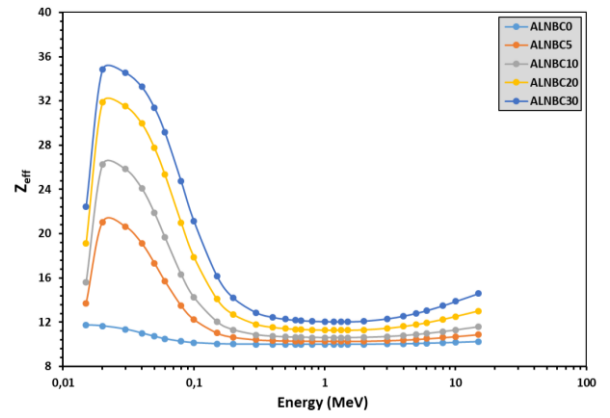

Figure 8 Z_{eff} values ALNBC composite samples

The theoretically calculated N_{eff} values for the ALNBC samples are presented in Figure 9.

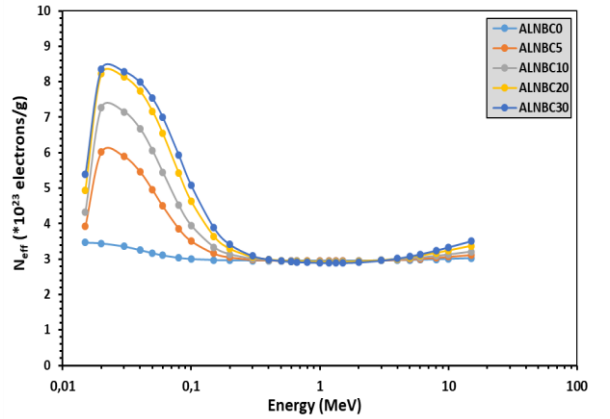

Figure 9 N_{eff} values ALNBC composite samples

An analysis of the N_{eff} results across all fabricated samples reveals a trend similar to that observed for the Z_{eff} over the studied photon energy ranges. However, unlike Z_{eff}, the N_{eff} values were found to range approximately between 3 and 9 x 10^{23}electrons per gram.

The theoretically calculated exposure buildup factor (EBF) values for the ALNBC samples are presented in Figure 10 as functions of photon energy and various penetration depths (1, 5, 10. 20. 30. and 40 mean free paths, MFPs). Overall, it was observed that EBF values decreased with increasing NbC content in the composites, indicating improved shielding performance due to the enhanced attenuation characteristics introduced by NbC.

As illustrated in Figure 10. the equivalent buildup factor (EBF) values exhibit a characteristic energy-dependent behavior. At lower photon energies, the EBF values remain relatively small, which is primarily due to the predominance of the photoelectric effect—a process that results in minimal secondary photon production. As the photon energy increases toward the intermediate range, the EBF values rise significantly. This increase is mainly driven by the onset of Compton scattering, which becomes the dominant interaction mechanism in this energy region and leads to enhanced generation of scattered (secondary) photons. At higher photon energies, particularly those exceeding the threshold of 1.022 MeV, a gradual decline in EBF values is observed. This reduction is associated with the increasing contribution of the pair production process, which, unlike Compton scattering, results in fewer scattered photons that contribute to buildup.

Moreover, at any given photon energy, EBF values were found to increase with increasing penetration depth. This behavior is consistent across all samples, with the highest EBF values recorded at 40 MFP, emphasizing the cumulative effect of multiple scattering events over greater material thicknesses

In this research article, the gamma radiation shielding performance of alumina (Al_2O_3) matrix composites reinforced with varying weight fractions of niobium carbide (NbC) was thoroughly examined through a combination of experimental measurements and theoretical simulations. Critical shielding parameters—LAC, MFP, HVL, TVL, RPE, Z_{eff}, N_{eff}, and EBF —were assessed across different photon energies and composite configurations. The experimental findings showed strong consistency with theoretical predictions generated using the Phy-X/PSD software, with relative deviation (RD) values ranging from 0.80% to 7.53%, indicating a high level of agreement within acceptable margins.

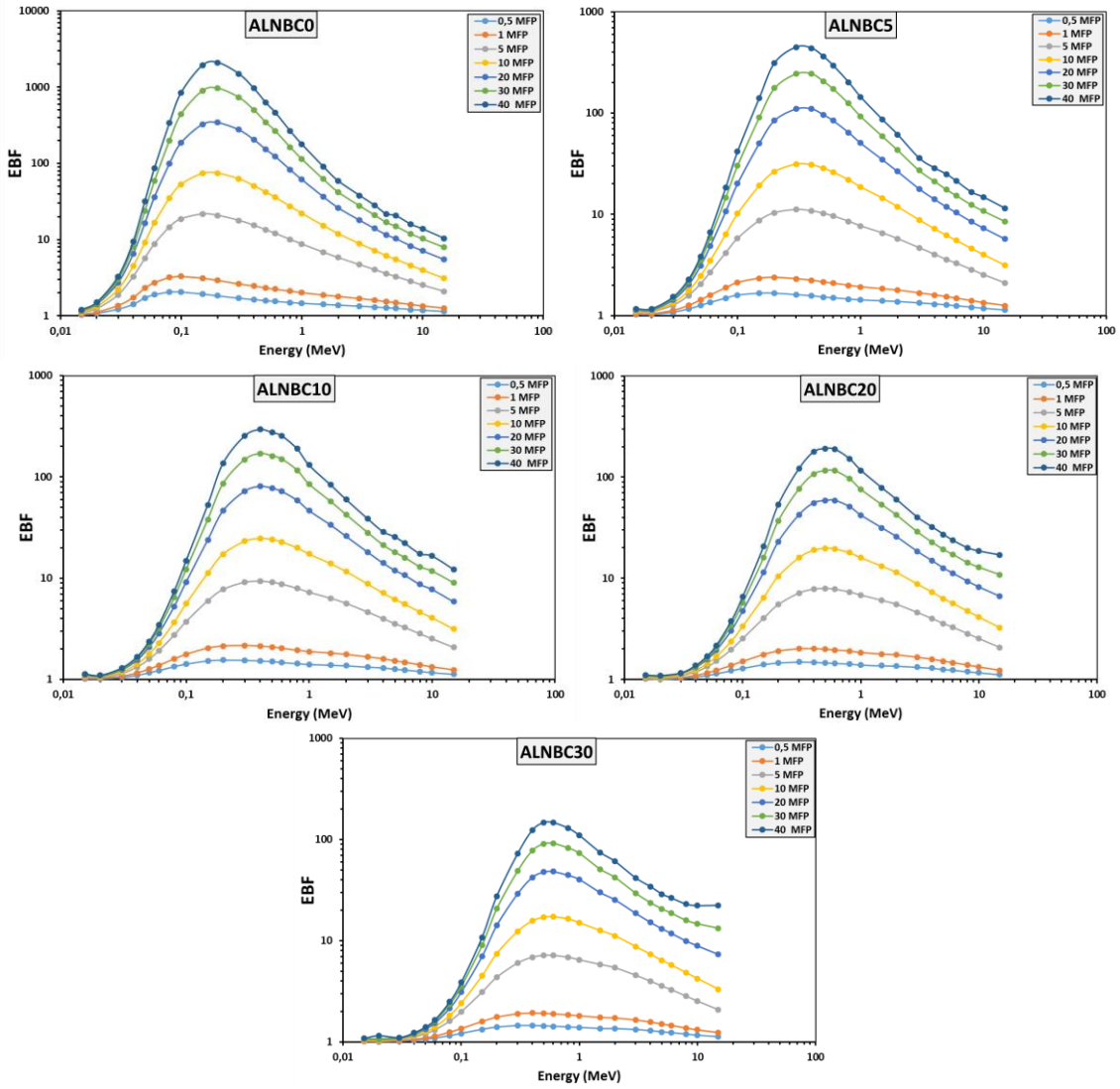

Figure 10 EBF values as a function of photon energy at 1, 5, 10. 20. 30 and 40 MFP (Phy-X/PSD).

Notably, the addition of NbC significantly improved the LAC values of the composites, particularly at lower photon energies. This enhancement is primarily attributed to the increased material density and effective atomic number resulting from the presence of NbC as a reinforcing agent, which contributes to more effective photon attenuation. Accordingly, the HVL, TVL, and MFP values were found to decrease with increasing NbC content, indicating improved attenuation capability and more compact shielding performance.

Furthermore, the RPE values increased with NbC loading and decreased with rising photon energy, highlighting the composite's effectiveness in low- and medium-energy gamma shielding. The calculated Z_{eff} and N_{eff} values also exhibited trends consistent with known photon interaction mechanisms—declining in the photoelectric-dominated low-energy region, stabilizing in the Compton-dominated mid-energy range, and increasing in the high-energy pair production region. The EBF values, which quantify secondary radiation buildup, were lowest in high-NbC samples and showed strong dependence on photon energy and penetration depth, with maximum values observed at 40 MFP.

Overall, the findings of this study confirm that NbC reinforcement substantially improves the radiation shielding effectiveness of alumina-based composites. These results suggest that ALNBC composites, particularly those with higher NbC content, are promising candidates for use in advanced gamma radiation shielding applications where both mechanical robustness and effective attenuation are required.

Declaration of Ethical Standards
The author declares compliance with all ethical standards.

Credit Authorship Contribution Statement
Author-1: References, Research, Experiment, Writing - original draft Visualisation, Writing - original draft

Declaration of Competing Interest
The author has no conflicts of interest to declare regarding the content of this article.

Data Availability Statement

The authors declare that all data generated or analyzed during this study are included in this published article

5. References

Afshar, M., Morshedian, J., Ahmadi, S., 2019. Radiation attenuation capability and flow characteristics of HDPE composite loaded with W, MoS2, and B4C, *Polymer Composites*, **40(1)**, 149–158. https://doi.org/10.1002/pc.24620

Ahammed, S., Echeweozo, E.O., Srinivas, B., Phani, A.L., Bhikshamaiah, G., Shareefuddin, M., Alomayrah, N., Al-Buriahi, M.S., 2024. Impact of NaF on electrical and radiation shielding properties of CdO-B2O3 glass system, *Journal of Radiation Research and Applied Sciences*, **17(4)** 101156. https://doi.org/10.1016/j.jrras.2024.101156

Akkurt, I., Altindag, R., Gunoglu, K., Sarıkaya, H., 2012. Photon attenuation coefficients of concrete including marble aggregates. *Annals of Nuclear Energy*, **43,** 56–60. https://doi.org/10.1016/j.anucene.2011.12.031

Akkurt, I., Gunoglu, K., 2021. Radiation shielding properties of concrete containing magnetite. *Progress in Nuclear Energy* **137,** 103776, 1-8. https://doi.org/10.1016/j.pnucene.2021.103776

Akman, F., Sayyed, M.I., Kaçal, M.R., Tekin H.O., 2019. Investigation of photon shielding performances of some selected alloys by experimental data, theoretical and MCNPX code in the energy range of 81 keV-1333 keV. Journal of Alloys and Compounds **772**, 516-524. https://doi.org/10.1016/j.jallcom.2018.09.177

Alzahrani, J.S., Alrowaili, Z.A., Eke, C., Mahmoud, Z.M.M., Mutuwong, C., Al-Buriahi, M.S., 2022. Nuclear shielding properties of Ni-, Fe-, Pb-, and W-based alloys. Radiation Physics and Chemistry **195,** 110090. https://doi.org/10.1016/j.radphyschem.2022.110090

AL Misned, G., Gunoglu, K., Varol Özkavak, H., Sen Baykal, D., Tekin, H.O., Karpuz N., Akkurt, I., 2023. An investigation on gamma-ray and neutron attenuation properties of multi-layered Al/B4C composite, *Materials Today Communications*, **36,** 106813. https://doi.org/10.1016/j.mtcomm.2023.106813

Al-Buriahi, M. S., Sayyed, M. I., Kaky, K. M., & Dong, M. 2021. Investigation of radiation shielding features of glass systems doped with heavy metal oxides. *Applied Radiation and Isotopes,* **169,** 109443. https://doi.org/10.1016/j.apradiso.2020.109443

Almuqrin, A.H., Jecong, J.F.M., Hila, F.C., Balderas, C.V., Sayyed, M.I., 2021. Radiation shielding properties of selected alloys using EPICS2017 data library, *Progress in Nuclear Energy,* **137** 103748. https://doi.org/10.1016/j.pnucene.2021.103748

Alsayed, Z., Badawi, M.S., Awad, R., El-Khatib, A.M., Thabet, A. A., 2020. Investigation of g-ray attenuation coefficients, effective atomic number and electron density for ZnO/HDPE composite, *Physica Scripta* **95,** https://doi.org/10.1088/ 1402-4896/ab9a6e

Alshahrani, B., Olarinoye, I.O., Mutuwong, C., Sriwunkum, C., Yakout, H.A., Tekin, H.O., Al-Buriahi, M.S., 2021. Amorphous alloys with high Fe content for radiation shielding applications, *Radiation Physics and Chemistry,* **183,** 109386. https://doi.org/10.1016/j.radphyschem.2021.109386

Alzahrani, J.S., Alrowaili, Z.A., Eke, C., Mahmoud, Z.M., Mutuwong, C., Al-Buriahi, M.S., 2022. Nuclear shielding properties of Ni-, Fe-, Pb-, and W-based alloys, *Radiation Physics and Chemistry* **195** 110090. https://doi.org/10.1016/j.radphyschem.2022.110090

Alzahrani, J.S., Alrowaili, Z.A., Mutuwong, C., Olarinoye, I.O., Al-Buriahi, M.S., 2023. Radiation shielding competence of chalcogenide alloys with high Te content, *Applied Radiation and Isotopes*, **196** 110759. https://doi.org/10.1016/j.apradiso.2023.110759

Ammar A. Oglat, Sabri M. Shalbi, 2022. An Alternative Radiation Shielding Material Based on Barium-Sulphate (BaSO4)-Modified Fly Ash Geopolymers. *Gels,* **8(4),** 227. https://doi.org/10.3390/gels8040227

ANSI/ANS-6.4.3, 1991. Gamma ray attenuation coefficient and buildup factors for engineering materials, *American Nuclear Society,* La Grange Park, Illinois

Atashi, P., Rahmani, S., Ahadi, B., Rahmati, A., 2018. Efficient, flexible and lead-free composite based on room temperature vulcanizing silicone rubber/W/Bi2O3 for gamma ray shielding application, *Journal of Materials Science: Materials in Electronics*, **29** 12306–12322. https://doi.org/10.1007/s10854-018-9344-1

Bashter, I.I., 1997. Calculation of radiation attenuation coefficients for shielding concretes. *Annals of Nuclear Energy* **24,** 1389. https://doi.org/10.1016/S0306-4549(97)00003-0

Gökmen U., Özkan Z., Jamalgolzari, L. E., Bilge Ocak S. 2020. Investigation of radiation attenuation properties of Al-Cu matrix composites reinforced by different amount of B_4C particles. Journal OF Boron **5(3)**,124–130. https://doi.org/10.30728/boron.730354

Gul, A. O., Kavaz, E., Basgoz, O., Guler, O., AL Misned, G., Bahceci, E., Albayrak, M.G., Tekin, H.O., 2022. Newly

synthesized NiCoFeCrW High-Entropy Alloys (HEAs): Multiple impacts of B4C additive on structural, mechanical, and nuclear shielding properties, *Intermetallics* **146,** 107593. https://doi.org/10.1016/j.intermet.2022.107593

Gunoglu K., Akkurt I., Sayyed, M. I., 2024. Radiation shielding properties of some igneous rocks in isparta province at different gamma energies: Experimental and theoretical study. *Journal of Radiation Research and Applied Sciences* **17,** 100796, 1-9. https://doi.org/10.1016/j.jrras.2023.100796

Gunoglu, K., 2024. Effect of colemanite mineral on gamma radiation attenuation properties of vinyl ester resin. *Journal of Radiation Research and Applied Sciences* **17** (2024) 100799, 1-7. https://doi.org/10.1016/j.jrras.2023.100799

Gunoglu, K., Varol Ozkavak, H., Akkurt, I., 2021. Evaluation of gamma ray attenuation properties of boron carbide (B4C) doped AISI 316 stainless steel: Experimental, XCOM and Phy-X/PSD database software. *Materials Today Communications* **29,** 102793, 1-9. https://doi.org/10.1016/j.mtcomm.2021.102793

Güler, S.H., Güler, O., Kavaz, E., Almisned, G., Issa, B., Tekin, H.O., 2024. Exploring critical behavioral differences in physical, structural, and nuclear radiation attenuation properties of produced High Entropy Alloy (HEA) and Refractory-High Entropy Alloy (RHEA) samples, *Current Applied Physics* **58,** 1–10. https://doi.org/ 10.1016/j.cap.2023.11.011

IAEA. 2018. Radiation Protection and Safety of Radiation Sources: International Basic Safety Standards (No. GSR Part 3). *International Atomic Energy Agency*. https://doi.org/10.61092/iaea.u2pu-60vm

Kaçal, M.R., Polat, H., Oltulu, M., Akman, F., Agar, O., Tekin, H.O., 2020. Gamma shielding and compressive strength analyses of polyester composites reinforced with zinc: an experiment, theoretical, and simulation based study, *Applied Physics A* **126** (3) 205. https://doi.org/10.1007/s00339-020-3382-2

Kaur, K.; Singh, K.; Anand, V. 2016. Structural properties of Bi2O3–B2O3–SiO2–Na2O glasses for gamma ray shielding applications. *Radiation Physics and Chemistry* **120.** 63–72. https://doi.org/10.1016/j.radphyschem.2015.12.003

Kilic, G., Ilik, E., Issa, S.A., Tekin, H.O., 2021. Synthesis and structural, optical, physical properties of Gadolinium (III) oxide reinforced TeO2–B2O3–(20-x) Li2O-xGd2O3 glass system, *Journal of Alloys and Compounds* **877,** 160302, https://doi.org/10.1016/j. jallcom.2021.160302

Kumar, A. 2017. Gamma ray shielding properties of PbO-Li2O-B2O3 glasses. *Radiation Physics and Chemistry* **136,** 50–53. https://doi.org/10.1016/j.radphyschem.2017.03.023

Li, H., Yan, L., Zhou, J., Wang, Y., Liao, X., Shi, B., 2024. Flexible and wearable functional materials for ionizing radiation Protection: A perspective review. Chemical Engineering Journal **487**, 150583. https://doi.org/10.1016/j.cej.2024.150583

Manjunatha, H.C., Sathish, K.V., Seenappa, L., Gupta, D., Raj, S. A. C., 2019. A study of X-ray, gamma and neutron shielding parameters in Si- alloys. Radiation Physics and Chemistry **165**, 108414. https://doi.org/10.1016/j.radphyschem.2019.108414

Mansour, M.A., Ismail, M.H.B., Imran Latif, Q.B.A., Alshalif, A.F., Milad, A., Bargi, W.A.A., 2023. A systematic review of the concrete durability incorporating recycled glass, *Sustainability* **15(4)** 3568. https://doi.org/10.3390/su15043568

Mansy, M. S., , Ghobashy, M. M., Aly M. I., 2024. Enhancing gamma and neutron radiation shielding efficiency of LDPE/PVC polymers using cobalt, aluminum, and magnesium oxide fillers. *Radiation Physics and Chemistry,* **222,** 111862. https://doi.org/10.1016/j.radphyschem.2024.111862

NCRP. 2000. Radiation Protection Guidance for Activities in Low-Earth Orbit, Report No. 132, ISBN : ISBN 0-929600-65-7

Oto, B., Çakar, N., Kavaz, E., Madak, Z., 2024. An experimental study on gamma radiation attenuation effectiveness of magnetite and serpentine doped ceramics, *Progress in Nuclear Energy* **169** 105079. https://doi.org/10.1016/j.pnucene.2024.105079

Rammah, Y.S., Olarinoye, I.O., El-Agawany, F.I., El-Adawy, A., 2020. Environment friendly La3+ions doped phosphate glasses/glass-ceramics for gamma radiation shielding: their potential in nuclear safety applications, *Ceramics International* **46(17)** 27616–27626. https://doi.org/10.1016/j.ceramint.2020.07.256

Sayyed, M. I., Kaur, P., Singh, D., & Matori, K. A. 2019. A comprehensive review on the radiation shielding properties of polymer composites. *Radiation Physics and Chemistry,* **166,** 108514. https://doi.org/10.1016/j.radphyschem.2019.108514

Singh, P.S., Singh, T., Kaur, P., 2008. Variation of energy absorption buildup factors with incident photon energy and penetration depth for some commonly used solvents. *Annals of Nuclear Energy*, **35(6),** 1093-1097.

https://doi.org/10.1016/j.anucene.2007.10.007

Şakar, E., Özpolat, Ö.F., Alım, B., Sayyed, M.I., Kurudirek, M., 2020. Phy-X/PSD: development of a user friendly online software for calculation of parameters relevant to radiation shielding and dosimetry. *Radiation Physics and Chemistry.* **166,** 108496. https://doi.org/10.1016/j.radphyschem.2019.108496

Tekin, H.O., Abouhaswa, A. S., Kilicoglu, O., Issa, S. A. M., Akkurt, I., Rammah, Y. S., 2020. Fabrication, physical characteristic, and gamma-photon attenuation parameters of newly developed molybdenum reinforced bismuth borate glasses, *Physica Scripta* **95,** 115703. https://doi.org/10.1088/1402-4896/abbf6e

Tekin, H.O., Issa, S.A., Ahmed, E.M., Rammah, Y.S., 2022. Lithium-fluoro borotellurite glasses: nonlinear optical, mechanical characteristics and gamma radiation protection characteristics, *Radiation Physics and Chemistry* **190.** 109819, https://doi.org/10.1016/j.radphyschem.2021.109819

Turhan, M.F., Akman, F., Taşer, A., Dilsiz, K., Oğul, H., Kacal, M.R., Agar, O., 2022. Gamma radiation shielding performance of CuxAg (1-x)-alloys: experimental, theoretical and simulation results, *Progress in Nuclear Energy* **143** 104036. https://doi.org/10.1016/j.pnucene.2021.104036

UNSCEAR 2010. Sources and Effects of Ionizing Radiation. United Nations Scientific Committee on the Effects of Atomic Radiation Report to the General Assembly. https://doi.org/10.18356/1b01bffb-en

Zayed, A.M., El-Khayatt, A.M., Petrounias, P., Shahien, M.G., Mahmoud, K.A., Rashad, A.M., Masoud, M.A., 2024. From discarded waste to valuable products: barite combination with chrysotile mine waste to produce radiation-shielding concrete, *Construction and Building Materials* **417** 135334. https://doi.org/10.1016/j.conbuildmat.2024.135334